

Original Article

# Residual Stress in Ceramic–Metal Tubes: Elastic–Ideally Plastic Model Analysis

Meriem Belhaou<sup>1</sup>, Nor eddine Laghzale<sup>2</sup>, Hakim Bouzid<sup>3</sup>

<sup>1,2</sup>ENSAM of Rabat, Mohammed V University in Rabat, Morocco.

<sup>3</sup>Mechanical Engineering Department, Ecole de Technologie Supérieure, Canada.

<sup>1</sup>Corresponding Author : [m.belhaou@um5r.ac.ma](mailto:m.belhaou@um5r.ac.ma)

Received: 15 June 2022

Revised: 05 September 2022

Accepted: 19 September 2022

Published: 30 September 2022

**Abstract** - An elastic-plastic analytical solution is developed using a prestressing method for a hollow cylinder made of a ceramic–metal functionally gradient material (FGM) under internal and external pressures to design a cylinder that resists plastic internal pressure efficiently uses the material at the outer part of the cylinder. Based on the experimental results for a ceramic–metal (Al A359/SiCp) cylinder produced with an FGM, different components of the radial, hoop, and axial stresses were analysed to investigate the effects of pressure, cylinder wall thickness, and material distribution. It is assumed that mechanical properties, such as Young's modulus and density, are governed by a power function along the wall thickness, owing to the functional gradation of the material. An elastic–perfectly plastic model and the von Mises criterion are used to obtain theoretical solutions for the stress distribution in the radial direction in the elastic and elastic–plastic areas and to determine different combinations of pressure. A finite element model was established to validate the analytical results by applying hypothetical thermal loads using Ansys Workbench. Thus, with an increasing ceramic volume fraction from the inner to outer radius, the reinforcement of the metal vessel by ceramic particles decreased the magnitude of the compressive hoop stresses at the inner section. It can improve the fatigue resistance and load-bearing capacity of the cylinder.

**Keywords** - Metal–ceramic, Functionally graded materials, Elastic–perfectly plastic, Pressurized hollow cylinders.

## 1. Introduction

Materials have played an essential role in developing modern industries and processes. The scientific use of basic materials in various organic and inorganic compounds has facilitated the development of advanced polymers, alloys, and structural engineering ceramics. It has led to the discovery of a new class of composite materials called functionally gradient materials (FGMs). FGMs are nonhomogeneous materials with continuously varying mechanical properties. They are unique materials that can operate in a harsh environment without losing their properties or deteriorating over time (Mahamood and Akinlabi 2017). Their main advantage is that their physical properties gradually vary according to the composition and microstructure of the material (Boggarapu et al., 2021; Pasha and Rajaprakash, 2022). These materials have been widely applied in various engineering and technology fields to achieve optimal use (Ibnorachid et al., 2021). An overview of the methods of manufacturing FGMs, describing the main advantages and disadvantages of these methods based on the literature for more than 30 years, is reported by Saleh et al. (2020).

In particular, ceramic–metal FGMs have potential applications in structures under severe operating conditions, including spacecraft heat shields (Bertolino et al. 2003; Zhang

et al. 2018), heat exchanger tubes (Hassanzadeh and Bilgili 2018), and plasma coatings in fusion reactors (Yan et al. 2010; Heuer et al. 2019). They are designed to reduce thermal stresses and utilise the heat resistance of ceramics and the mechanical strength and good machinability of metals without significant internal thermal stress (Chmielewski and Pietrzak 2016; Ruys and Sutton 2021). Although the concept of ceramic–metal FGMs was initially proposed for super-heat-resistant materials, FGM pressure vessels have attracted attention because of their excellent mechanical properties.

The mechanical behaviours of FGM pressure vessels and cylinders subjected to internal pressure have been investigated extensively using different Young's modulus functions (Ruys and Sutton 2021; Tutuncu and Ozturk 2001; Sburlati 2012; Benslimane et al. 2021; Chen and Lin 2008; Shi et al. 2007; Benslimane et al. 2018). Tutuncu and Ozturk (2001), Sburlati (2012) and Benslimane et al. (2021) analysed an elastic, linear, isotropic, compressible FGM cylinder using a power law Young's modulus. Chen and Lin (2008) derived an exponential function to represent Young's modulus for elastic analysis of thick cylinders and spherical pressure vessels made of FGMs. Shi et al. (2007) used a linear function to represent Young's modulus of an FGM cylinder under pressure. In more complex cases, researchers have assumed that Young's



modulus varies according to a general nonlinear expression (Benslimane et al., 2018). Studies have shown the effect of the gradient index on elastic solutions of a thick-walled pressurised cylinder made of an FGM and the effect of Poisson's ratio on the latter (Mognhod and Engida 2021).

However, in these studies, the analyses were limited to elastic fields. This study was based on the numerical method used in the elastic domain in Sburlati (2012). The aim is to adapt it to a cylinder made of an FGM plastically deformed under internal and external pressures to obtain optimal solutions.

To reflect both elastic and plastic effects, Eraslan and Akis (2005) and Xin et al. (2016) obtained analytical solutions of stresses and radial displacements for the plastic analysis of a functionally graded thick-walled tube subjected to internal pressure. Thick-walled cylinders are typically subjected to extremely high pressures and thermal loads during their lifetimes. Therefore, several numerical methods have been used to evaluate the thermo-elasto-plastic behaviour of a thick-walled cylinder made of an FGM. Nayak et al. (2020) studied the elasto-plastic properties of thermomechanically loaded functionally graded (FG) disks using an iterative variational method. The response of an FG disk with arbitrary material composition in the radial direction under thermo-mechanical loads was investigated using the differential transformation method (Heydari 2019) and successive approximation method (Saeedi et al. 2021). Considering the rotation effect, Benchallal et al. (2022) derived an exact analytical closed-form solution from the governing equations to compute the thermo-mechanical stress field for a rotating hollow cylinder made of FGMs subjected to internal pressure and uniform temperature. In the references cited above, using the modified mixing rule, the effective material properties were based on the two-phase volumetric fraction in the graded direction. Sim et al. (2021) developed a recursive algorithm to formulate an analytical solution for the thermo-elastic behaviour of a multilayered spherical pressure vessel.

In these studies, advanced numerical methods were applied to solve complex problems, particularly for analysing the behaviour of the material or boundary conditions. However, these studies were limited to identifying the effect of material properties on the responses of stress, strain, and displacement profiles in thick-walled FGM cylinders under mechanical and thermal loads. This study aims to investigate the elasto-plastic response of stress in a pressurised FGM cylinder and the residual stress. It is well known that internal-compressive residual stresses are generated after the pressure is released during prestressing techniques (Cui et al. 2021; Zheng et al. 2021; Mohan et al. 2020, 2021), such as autofrettage (Mohan et al. 2021).

During the loading phase of the autofrettage process, a large part of the cylinder deforms plastically. When the load is removed, the inner part of the vessel develops compressive residual stresses, whereas the outer part develops tensile residual stresses. The inner part of the vessel is subjected to compressive residual stress, which improves the vessel's fatigue strength and load-bearing capacity (Molaie et al. 2018), resulting in a longer service life under cyclic internal pressure.

This study aims to determine the optimal autofrettage pressure and associated elastoplastic boundary radius for metal-ceramic FGM cylinders. To date, no experimental studies have been conducted on the elastoplastic analysis of actual metal or ceramic cylinders under internal and external pressure loads. This analysis reflected the experimental findings of Rodríguez-Castro (2002) for an FG Al A359/SiCp cylinder. In a metal cylinder, the residual compressive stresses generated during autofrettage are typically constrained by the plasticity of the metal. The properties of a homogenised Al A359 steel cylinder and an Al A359/SiCp cylinder were compared to demonstrate the advantages of an FGM and to support the current study. Based on the von Mises yield criterion, different components of the radial, hoop, and normal stresses are presented to analyse the effects of pressure, cylinder wall thickness, and material distribution. They were obtained in the cylinder's elastic, elastoplastic, and fully plastic zones. Finally, explicit analytical formulas for the residual elastic stress within the tube wall were derived based on the classical elastic-ideally, plastic solution, neglecting the Bauschinger effect. The optimal stress distribution, optimal autofrettage pressure, and optimal thickness were obtained. However, despite the lack of analysis software, it does not directly model the variation in Young's modulus as a space function. A numerical study using the finite element method in Ansys Workbench was conducted. The analytical model's solutions were then compared with the numerical solutions.

## 2. Materials and Methods

### 2.1. Material Behavior and Geometry Characteristics

An axisymmetric infinitely long cylinder is analysed. It is made of a metal-ceramic FGM with an inner radius  $R_i$  and an outer radius  $R_o$ . The hollow cylinder is subjected to internal pressure  $P_i$  and external pressure  $P_o$ . Poisson's ratio  $\nu$  is assumed to be constant. Finally, Young's modulus  $E(r)$  and yield stress  $\sigma_y(r)$  are power-law functions, expressed as follows, respectively:

$$E(r) = E_i \left( \frac{r}{R_i} \right)^n \quad (1)$$

$$\sigma_y(r) = \sigma_i \left( \frac{r}{R_i} \right)^m \quad (2)$$

where  $r$  is the radius,  $n$  and  $m$  are material parameters.  $E_i$  and  $\sigma_i$  are Young's modulus and yield stress at the inner radius  $r = R_i$ .

A schematic of the pressurized hollow cylinder is shown in Fig. 1.

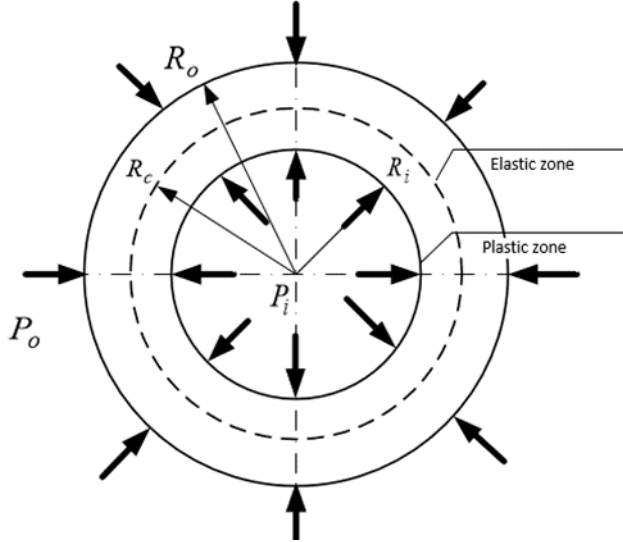


Fig. 1 The drawing of the ceramic/metal hollow cylinder under internal and external pressure.

2.2. Loading Stress Analysis

2.2.1. Elastic stress analysis

The hollow cylinder is purely elastic, and the stress-controlled boundary conditions are defined as follows.

$$\sigma_r|_{r=R_i} = -P_i, \sigma_r(r)|_{r=R_o} = -P_o \tag{3}$$

Based on these conditions, stress equations (4)–(5) can be written as follows (Sburlati 2012):

$$\sigma_r(r) = \frac{R_i^{-\frac{n}{2}+1} r^{\frac{n}{2}-1}}{\left(Y^{-\frac{k}{2}} - Y^{\frac{k}{2}}\right)} \left[ \left(\frac{r}{R_o}\right)^{-\frac{k}{2}} - \left(\frac{r}{R_o}\right)^{\frac{k}{2}} \right] P_i - \frac{R_o^{-\frac{n}{2}+1} r^{\frac{n}{2}-1}}{\left(Y^{-\frac{k}{2}} - Y^{\frac{k}{2}}\right)} \left[ \left(\frac{r}{R_i}\right)^{-\frac{k}{2}} - \left(\frac{r}{R_i}\right)^{\frac{k}{2}} \right] P_o \tag{4}$$

$$\sigma_\theta(r) = \frac{R_i^{-\frac{n}{2}+1} r^{\frac{n}{2}-1}}{\left(Y^{-\frac{k}{2}} - Y^{\frac{k}{2}}\right)} \left[ \left(\frac{r}{R_o}\right)^{-\frac{k}{2}} \left(\frac{n-k}{2}\right) - \left(\frac{r}{R_o}\right)^{\frac{k}{2}} \left(\frac{n+k}{2}\right) \right] P_i - \frac{R_o^{-\frac{n}{2}+1} r^{\frac{n}{2}-1}}{\left(Y^{-\frac{k}{2}} - Y^{\frac{k}{2}}\right)} \left[ \left(\frac{r}{R_i}\right)^{-\frac{k}{2}} \left(\frac{n-k}{2}\right) - \left(\frac{r}{R_i}\right)^{\frac{k}{2}} \left(\frac{n+k}{2}\right) \right] P_o \tag{5}$$

$$\sigma_z(r) = \frac{\nu R_i^{-\frac{n}{2}+1} r^{\frac{n}{2}-1}}{\left(Y^{-\frac{k}{2}} - Y^{\frac{k}{2}}\right)} \left[ \left(\frac{r}{R_o}\right)^{-\frac{k}{2}} \left(\frac{2+n-k}{2}\right) - \left(\frac{r}{R_o}\right)^{\frac{k}{2}} \left(\frac{2+n+k}{2}\right) \right] P_i - \frac{\nu R_o^{-\frac{n}{2}+1} r^{\frac{n}{2}-1}}{\left(Y^{-\frac{k}{2}} - Y^{\frac{k}{2}}\right)} \left[ \left(\frac{r}{R_i}\right)^{-\frac{k}{2}} \left(\frac{2+n-k}{2}\right) - \left(\frac{r}{R_i}\right)^{\frac{k}{2}} \left(\frac{2+n+k}{2}\right) \right] P_o \tag{6}$$

where  $k$  is defined by Sburlati (2012) as follows:

$$k = -\sqrt{n^2 + 4 - \frac{4n\nu}{1-\nu}} \tag{7}$$

Furthermore, if  $n = 0$  the tube is homogeneous, Eqs. (2) and (3) reduce to the well-known equations derived by Vullo (2013).

2.2.2. Elastic-plastic stress analysis

For a hollow cylinder composed of homogeneous materials, the elastic limit pressure,  $P_{lim}$ , exists  $r = R_i$  (Laghzale and Bouzid 2016). However, the plasticity of an FGM hollow cylinder begins from either the inner or outside surfaces (Kalali and Hadidi-Moud 2013). For an Al A359/SiCp FG cylinder, the elastic part of the cylinder is considered to be under inside and outside pressures while reaching the yield at its inside radius.

The von Mises equivalent stress is expressed as follows (Laghzale and Bouzid 2016).

$$\sigma_{eq} = \frac{\sqrt{3}}{2} (\sigma_\theta - \sigma_r) \tag{8}$$

Applying the von Mises yield criterion at  $r = R_i$  yields Eq. (9).

$$\sigma_{eq}(r)|_{r=R_i} = \sigma_y(r)|_{r=R_i} \tag{9}$$

By substituting Eqs. (4) and (5) into Eq. (9), the elastic limit pressure  $r = R_i$  is defined by Eq. (10)

$$P \frac{4\sigma_i}{\sqrt{3}} \frac{\left(Y^{-\frac{k}{2}} - Y^{\frac{k}{2}}\right)}{Y^{\frac{k}{2}(n-k-2)} + Y^{-\frac{k}{2}(2-n-k)}} \lim - Y^{-\frac{n}{2}+1} \cdot 2 \cdot k \cdot P_o \tag{10}$$

When internal pressure  $P_i$  increases beyond the yield point, a zone of total plasticity of radius ( $R_c$ ) develops as a function of the increase in the internal pressure in the cylinder. It results in the appearance of a plastic zone and an elastic zone.

The equilibrium equation is expressed as follows (Laghzale and Bouzid 2016).

$$\frac{d\sigma_r}{dr} = \frac{2}{\sqrt{3}} \frac{\sigma_{eq}}{r} \tag{11}$$

The material was assumed to be non-work-hardened. In this case, the stresses in the plastic zone are determined as follows by integrating Eq. (11) between and using Eq. (2).

$$\sigma_r(r) = \frac{2}{\sqrt{3}} \sigma_i \left[ \frac{1}{m} \left( \frac{r}{R_i} \right)^m + C \right] \tag{12}$$

$$\sigma_\theta(r) = \frac{2}{\sqrt{3}} \sigma_i \left[ \left( \frac{1}{m} + 1 \right) \left( \frac{r}{R_i} \right)^m + C \right] \tag{13}$$

As the plastic region reaches the radius  $R_c$  (Fig. 2), the following boundary conditions apply.

$$\sigma_r(r)|_{r=R_c}^{plastic} = \sigma_r(r)|_{r=R_c}^{elastic} = -P_c \tag{14}$$

The constant  $C$ , is obtained, and the stresses in the plastic zone are determined as follows.

$$\sigma_r(r) = \frac{2}{\sqrt{3}} \frac{1}{m} \sigma_i \left[ \left( \frac{r}{R_i} \right)^m - \left( \frac{R_c}{R_i} \right)^m \right] - P_c \tag{15}$$

$$\sigma_\theta(r) = \frac{2}{\sqrt{3}} \sigma_i \left[ \left( \frac{1}{m} + 1 \right) \left( \frac{r}{R_i} \right)^m - \frac{1}{m} \left( \frac{R_c}{R_i} \right)^m \right] - P_c \tag{16}$$

By applying the von Mises yield criterion at  $r = R_c$ , Eq. (17) is derived.

$$\sigma_{eq}(r)|_{r=R_c} = \sigma_y(r)|_{r=R_c} \tag{17}$$

The critical pressure at the elastic-plastic interface  $r = R_c$  is expressed as follows.

$$P_c = \frac{4\sigma_i}{\sqrt{3}} \cdot \frac{\left( \frac{R_c}{R_i} \right)^m \left( Y_c^{-\frac{k}{2}} - Y_c^{\frac{k}{2}} \right)}{Y_c^{\frac{k}{2}} \cdot (n-k-2) + Y_c^{-\frac{k}{2}} \cdot (2-n-k)} - Y_c^{-\frac{n}{2}+1} \cdot 2 \cdot k \cdot P_o \tag{18}$$

By substituting Eqs. (17) into Eqs. (15) and (16), the radial and hoop stress distributions at any position ( $r$ ) and for different values of ( $R_c$ ) are expressed as follows.

$$\sigma_r(r) = \frac{2}{\sqrt{3}} \frac{1}{m} \sigma_i \left[ \left( \frac{r}{R_i} \right)^m - \left( \frac{R_c}{R_i} \right)^m \right] - \frac{4\sigma_i}{\sqrt{3}} \cdot \frac{\left( \frac{R_c}{R_i} \right)^m \left( Y_c^{-\frac{k}{2}} - Y_c^{\frac{k}{2}} \right)}{Y_c^{\frac{k}{2}} \cdot (n-k-2) + Y_c^{-\frac{k}{2}} \cdot (2-n-k)} + Y_c^{-\frac{n}{2}+1} \cdot 2 \cdot k \cdot P_o \tag{19}$$

$$\sigma_\theta(r) = \frac{2}{\sqrt{3}} \sigma_i \left[ \left( \frac{1}{m} + 1 \right) \left( \frac{r}{R_i} \right)^m - \frac{1}{m} \left( \frac{R_c}{R_i} \right)^m \right] - \frac{4\sigma_i}{\sqrt{3}} \cdot \frac{\left( \frac{R_c}{R_i} \right)^m \left( Y_c^{-\frac{k}{2}} - Y_c^{\frac{k}{2}} \right)}{Y_c^{\frac{k}{2}} \cdot (n-k-2) + Y_c^{-\frac{k}{2}} \cdot (2-n-k)}$$

$$+ Y_c^{-\frac{n}{2}+1} \cdot 2 \cdot k \cdot P_o \tag{20}$$

2.2.3. Fully Plastic Stress Analysis

The cylinder becomes fully plastic when  $R_c$  it becomes equal to the outer radius  $R_o$ . In this case, the pressure  $P_p$  required to plasticise the entire cylinder is determined by considering the radial stress expressed by Eq. (15) at an outer radius equal to Eq. (22).

$$\sigma_r(r)|_{r=R_o} = -P_o \tag{22}$$

$$P_p = \frac{4\sigma_i}{\sqrt{3}} \cdot \frac{Y^m \left( Y^{-\frac{k}{2}} - Y^{\frac{k}{2}} \right)}{\left( Y^{\frac{k}{2}} \cdot (n-k-2) + \left( Y \right)^{-\frac{k}{2}} \cdot (2-n-k) \right) - \left( Y \right)^{-\frac{n}{2}+1} \cdot 2 \cdot k \cdot P_o - \frac{2}{\sqrt{3}} \cdot \frac{1}{m} \cdot \sigma_i \cdot (1 - Y^m)} \tag{23}$$

Therefore, the stresses in a fully plastic cylinder are determined using Eq. (24).

$$\sigma_r(r) = \frac{2}{\sqrt{3}} \frac{1}{m} \sigma_i \left[ \left( \frac{r}{R_i} \right)^m - Y^m \right] - P_i \tag{24}$$

$$\sigma_\theta(r) = \frac{2}{\sqrt{3}} \sigma_i \left[ \left( \frac{1}{m} + 1 \right) \left( \frac{r}{R_i} \right)^m - \frac{1}{m} Y^m \right] - P_i \tag{25}$$

2.3. Autofrettage Process

2.3.1. Autofrettage Pressure

By applying the stress-controlled boundary conditions in Eqs. (2), the autofrettage pressure  $P_i$ , is obtained from the numerical solution of the following nonlinear equation.

$$P_i = \frac{4\sigma_i}{\sqrt{3}} \cdot \frac{\left( \frac{R_c}{R_i} \right)^m \left( \left( \frac{R_o}{R_c} \right)^{-\frac{k}{2}} - \left( \frac{R_o}{R_c} \right)^{\frac{k}{2}} \right)}{\left( \frac{R_o}{R_c} \right)^{\frac{k}{2}} \cdot (n-k-2) + \left( \frac{R_o}{R_c} \right)^{-\frac{k}{2}} \cdot (2-n-k)} - \left( \frac{R_o}{R_c} \right)^{-\frac{n}{2}+1} \cdot 2 \cdot k \cdot P_o - \frac{2}{\sqrt{3}} \cdot \frac{1}{m} \cdot \sigma_i \cdot \left[ 1 - \left( \frac{R_c}{R_i} \right)^m \right] \tag{21}$$

When the autofrettage pressure is completely removed, unloading pressure  $P^*$  equals  $P_i$ . Unloading is perfectly elastic. There is no reverse yielding. The elastic unloading process is analysed using  $P^* > P_{lim}$ . The stresses expressed by Eqs. (18) and (19) are modified by subtracting the solution for the purely elastic stresses expressed by Eqs. (4) and (5) such that the final residual stresses are as follows.

Plastic loading and elastic unloading zone ( $R_i \leq r \leq R_c$ ):

$$\begin{aligned} \sigma_r^R(r) = & \frac{2}{\sqrt{3}} \frac{1}{m} \sigma_i \left[ \left( \frac{r}{R_i} \right)^m - \left( \frac{R_c}{R_i} \right)^m \right] - \frac{4\sigma_i}{\sqrt{3}} \cdot \\ & \frac{\left( \frac{R_c}{R_i} \right)^m \left( Y_c^{-\frac{k}{2}} - Y_c^{\frac{k}{2}} \right)}{Y_c^{\frac{k}{2}} \cdot (n-k-2) + Y_c^{-\frac{k}{2}} \cdot (2-n-k)} + Y_c^{-\frac{n}{2}+1} \cdot 2.k.P_o \\ & - \frac{R_i^{-\frac{n}{2}+1} r^{\frac{n}{2}-1}}{\left( Y_c^{-\frac{k}{2}} - Y_c^{\frac{k}{2}} \right)} \left[ \left( \frac{r}{R_0} \right)^{\frac{k}{2}} - \left( \frac{r}{R_0} \right)^{\frac{k}{2}} \right] P^* \\ & + \frac{R_0^{-\frac{n}{2}+1} r^{\frac{n}{2}-1}}{\left( Y_c^{-\frac{k}{2}} - Y_c^{\frac{k}{2}} \right)} \left[ \left( \frac{r}{R_i} \right)^{\frac{k}{2}} - \left( \frac{r}{R_i} \right)^{\frac{k}{2}} \right] P_0 \end{aligned} \tag{26}$$

$$\begin{aligned} \sigma_\theta^R(r) = & \frac{2}{\sqrt{3}} \sigma_i \left[ \left( \frac{1}{m} + 1 \right) \left( \frac{r}{R_i} \right)^m - \frac{1}{m} \left( \frac{R_c}{R_i} \right)^m \right] - \frac{4\sigma_i}{\sqrt{3}} \cdot \\ & \frac{\left( \frac{R_c}{R_i} \right)^m \left( Y_c^{-\frac{k}{2}} - Y_c^{\frac{k}{2}} \right)}{Y_c^{\frac{k}{2}} \cdot (n-k-2) + Y_c^{-\frac{k}{2}} \cdot (2-n-k)} + Y_c^{-\frac{n}{2}+1} \cdot 2.k.P_o \\ & - \frac{R_i^{-\frac{n}{2}+1} r^{\frac{n}{2}-1}}{\left( Y_c^{-\frac{k}{2}} - Y_c^{\frac{k}{2}} \right)} \left[ \left( \frac{r}{R_0} \right)^{\frac{k}{2}} \left( \frac{n-k}{2} \right) - \left( \frac{r}{R_0} \right)^{\frac{k}{2}} \left( \frac{n+k}{2} \right) \right] P^* \\ & + \frac{R_0^{-\frac{n}{2}+1} r^{\frac{n}{2}-1}}{\left( Y_c^{-\frac{k}{2}} - Y_c^{\frac{k}{2}} \right)} \left[ \left( \frac{r}{R_i} \right)^{\frac{k}{2}} \left( \frac{n-k}{2} \right) - \left( \frac{r}{R_i} \right)^{\frac{k}{2}} \left( \frac{n+k}{2} \right) \right] P_0 \end{aligned} \tag{27}$$

Elastic loading and unloading zone ( $R_c \leq r \leq R_o$ ):

$$\begin{aligned} \sigma_r^R(r) = & r^{\frac{n}{2}-1} \left[ \left( \frac{r}{R_0} \right)^{\frac{k}{2}} - \left( \frac{r}{R_0} \right)^{\frac{k}{2}} \right] P_i \\ & \cdot \left[ \frac{R_c^{-\frac{n}{2}+1}}{\left( Y_c^{-\frac{k}{2}} - Y_c^{\frac{k}{2}} \right)} - \frac{R_i^{-\frac{n}{2}+1}}{\left( Y_c^{-\frac{k}{2}} - Y_c^{\frac{k}{2}} \right)} \right] - R_0^{-\frac{n}{2}+1} r^{\frac{n}{2}-1} P_0 \\ & \left[ \frac{\left( \frac{r}{R_c} \right)^{\frac{k}{2}} - \left( \frac{r}{R_c} \right)^{\frac{k}{2}}}{\left( Y_c^{-\frac{k}{2}} - Y_c^{\frac{k}{2}} \right)} - \frac{\left( \frac{r}{R_i} \right)^{\frac{k}{2}} - \left( \frac{r}{R_i} \right)^{\frac{k}{2}}}{\left( Y_c^{-\frac{k}{2}} - Y_c^{\frac{k}{2}} \right)} \right] \end{aligned} \tag{28}$$

$$\begin{aligned} \sigma_\theta^R(r) = & r^{\frac{n}{2}-1} \left[ \left( \frac{r}{R_0} \right)^{\frac{k}{2}} \left( \frac{n-k}{2} \right) - \left( \frac{r}{R_0} \right)^{\frac{k}{2}} \left( \frac{n+k}{2} \right) \right] P_i \\ & \cdot \left[ \frac{R_c^{-\frac{n}{2}+1}}{\left( Y_c^{-\frac{k}{2}} - Y_c^{\frac{k}{2}} \right)} - \frac{R_i^{-\frac{n}{2}+1}}{\left( Y_c^{-\frac{k}{2}} - Y_c^{\frac{k}{2}} \right)} \right] - R_0^{-\frac{n}{2}+1} r^{\frac{n}{2}-1} P_0 \\ & \left[ \frac{\left( \frac{r}{R_c} \right)^{\frac{k}{2}} \left( \frac{n-k}{2} \right) - \left( \frac{r}{R_c} \right)^{\frac{k}{2}} \left( \frac{n+k}{2} \right)}{\left( Y_c^{-\frac{k}{2}} - Y_c^{\frac{k}{2}} \right)} - \frac{\left( \frac{r}{R_i} \right)^{\frac{k}{2}} \left( \frac{n-k}{2} \right) - \left( \frac{r}{R_i} \right)^{\frac{k}{2}} \left( \frac{n+k}{2} \right)}{\left( Y_c^{-\frac{k}{2}} - Y_c^{\frac{k}{2}} \right)} \right] \end{aligned} \tag{29}$$

When the operating pressure is applied, the total stress of the partially autofrettaged cylinder becomes the sum of the residual stress and the stress generated by the operating pressure; that is,

$$\begin{aligned} \sigma_r^T &= \sigma_r + \sigma_r^R \\ \sigma_\theta^T &= \sigma_\theta + \sigma_\theta^R \end{aligned} \tag{30}$$

2.3.2. Optimal Autofrettage Pressure

The cylinder is expected to be under high internal pressure during operations; therefore, we employ the autofrettage process to increase the pressure-bearing capacity of the cylinder before use. An approach is defined by Molaie et al. (2018) under working conditions to determine the optimal level of autofrettage, and minimal hoop stress is generated. The various states of the total hoop stress, depending on the autofrettage pressure levels, were plotted together. The angled points on each curve indicate the elasto-plastic boundary, which must be shown. The maximum point of each curve indicates the total hoop stress  $R_c$ . Hence, the envelope curve is defined as follows (Molaie et al. 2018).

$$f(Y_c) = \sigma_\theta^R(Y_c) + \left[ \frac{R_i^{\frac{n+1}{2}} r^{\frac{n-1}{2}}}{Y_c^{\frac{k}{2}} - Y_c^{\frac{k}{2}}} \right] \left[ (r)^{\frac{k}{2}} \left( \frac{n-k}{2} \right) - (r)^{\frac{k}{2}} \left( \frac{n+k}{2} \right) \right] P_w \tag{31}$$

3. Results and Discussion

In this study, an elastic-plastic stress analysis was performed for a hollow cylinder made of ceramic-metal FGMs under internal and external pressures Using analytical and numerical methods. Axisymmetric elements were used to model and mesh the cylinder in Ansys for the numerical method (Bist and Bhatt, 2021). Ansys enables the description of attributes that depend on temperature; in particular, one can assign temperature values that depend on position. These two scenarios act simultaneously to make the material quality dependent on the position. The effect of temperature was neglected in this study. For an Al A359/SiCp FG material with various SiC volume fractions, Rodriguez-Castro et al. (2002) reported the experimental data presented in Fig. 2.

The cylinder was made of an FGM; an aluminium-alloy matrix reinforced with silicon carbide particles at 30% of the inner surface and 20% of the outer surface (Rodríguez-Castro et al. 2002). The geometrical and mechanical properties of the cylinder are listed in Table I using data extracted from Parvizi et al. (2011).

Table 1. Geometrical and mechanical characteristics (Parvizi et al. 2011)

$R_i$ (mm)	$R_o$ (mm)	$E_i$ (GPa)	$\sigma_i$ (MPa)	$n$	$m$
20	40	108.97	93.06	-0.28	-0.28

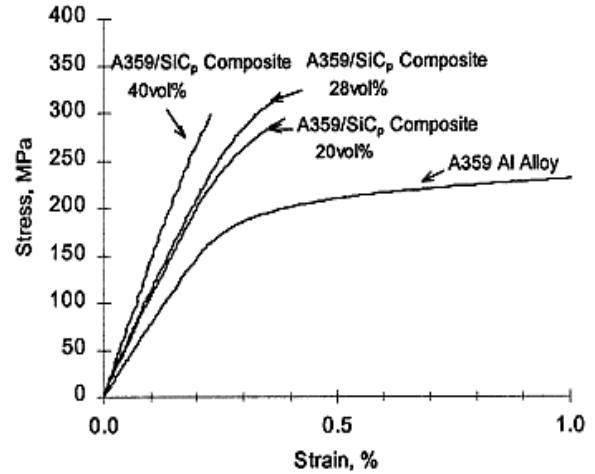
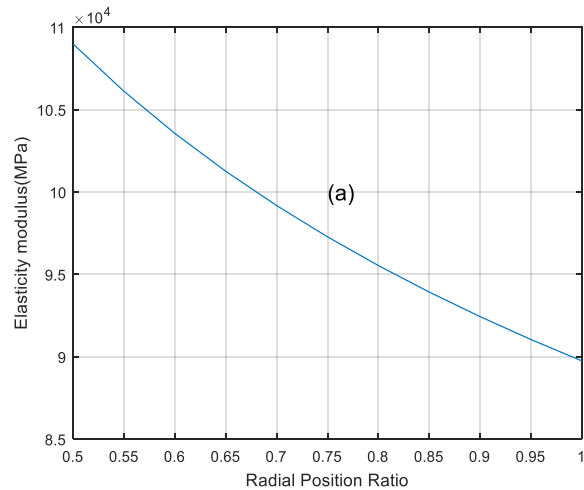


Fig. 2 Stress–strain curves for monolithic Al A359 alloy and Al A359/SiCp composite at different volume fraction (Rodríguez-Castro et al. 2002)

Fig. 2 shows the variations in the elasticity modulus  $E(r)$  (a) and yielding stress  $\sigma_y(r)$  (b) in the radial direction of the FG Al A359/SiCp cylinder.  $E$  and  $\sigma_y$  were assumed to exhibit similar variations, as shown in Fig. 2. However, they varied at different rates. The values of  $E$  and  $\sigma_y$  decreased from the inner surface to the outer surface. These variations were also observed in the numerical (Ansys) solutions.



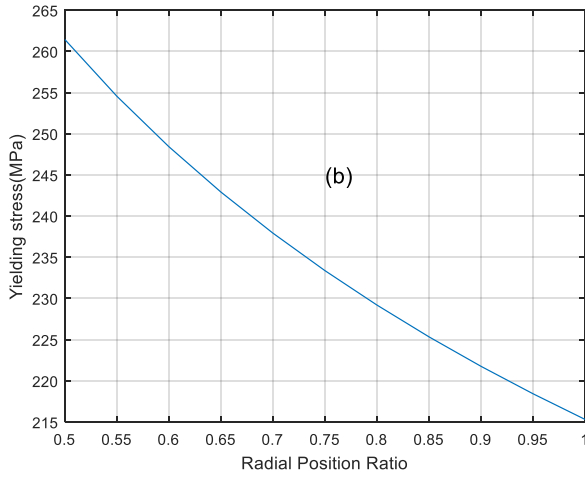


Fig. 3 Variations of the (a) elasticity modulus and (b) yielding stress.

Figs. 4–7 show the variations in the radial, hoop, normal, and equivalent stresses in elastic, elasto-plastic, and fully plastic cases. In the elastic case  $P_i < P_{lim}$ , all the stresses reach their maximum at the inner surface of the cylinder. The radial stress is always compressive, as it has negative values in all three cases. However, the hoop stress always has a positive value and represents the tensile stress. In the elasto-plastic case, as the pressure increases above the elastic limit  $P_i > P_{lim}$ , the plastic zone of radius ( $r$ ) propagates, and the maximum of the hoop, normal, and equivalent stresses relocate from the bore of the cylinder to half the thickness of the cylinder ( $R_c/R_o = 0.75$ ) and then decrease in the elastic zone. For the fully plastic condition  $P_i = P_p$ , the stresses increase through the entire cylinder thickness, with the maximum stress at the outside radius.

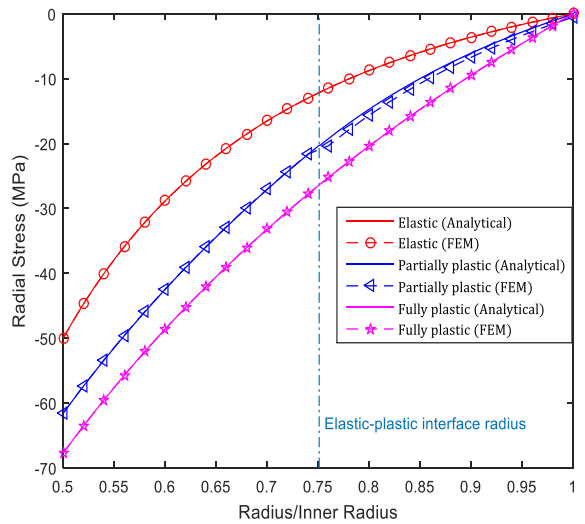


Fig. 4 Variations of the elastic, elastic-plastic and fully plastic radial stress in a FG Al A359/ SiCp cylinder.

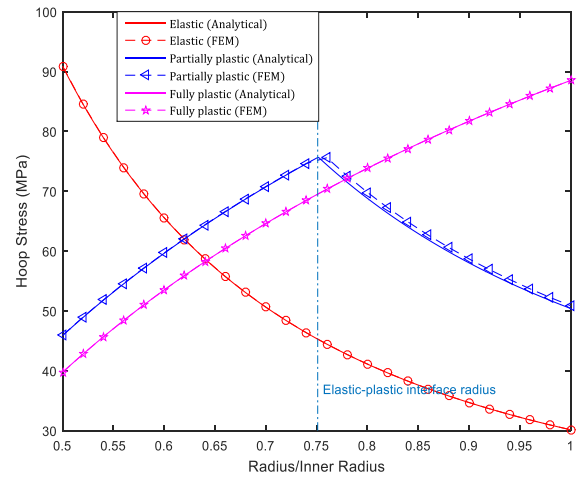


Fig. 5 Variations of elastic, plastic, and fully plastic hoop stress in a FG Al A359/ SiCp cylinder.

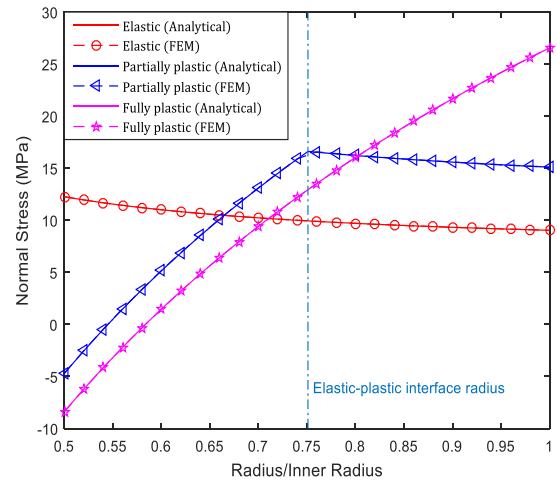


Fig. 6 Variations of the elastic, elastic-plastic and fully plastic normal stress in an FG Al A359/ SiCp cylinder.

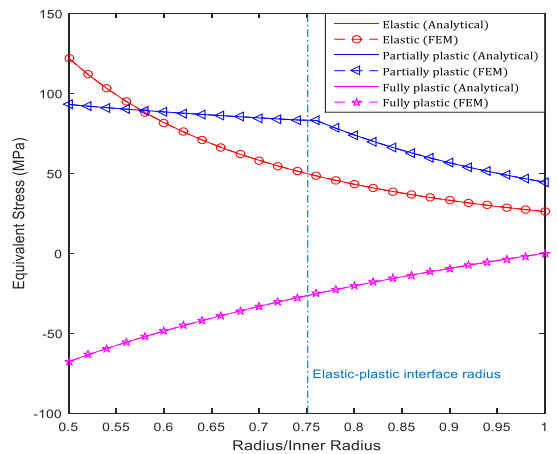


Fig. 7 Variations of the elastic, elastic-plastic and fully plastic equivalent stress in an FG Al A359/ SiCp.

Fig. 8 shows the results for several values of  $(R_o/R_c)$ . The hoop stress increases as a function of the widening of the radius of plasticity  $R_c$ , particularly at  $R_c = R_o$ . Hence, the existence of a pressure difference explains the presence of residual stresses.

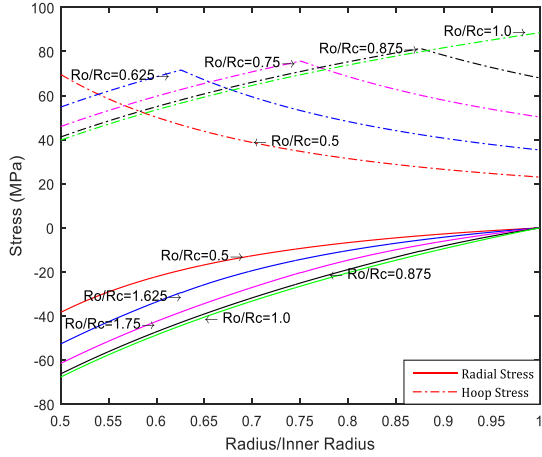


Fig. 8 Variations of radial and hoop stress in an FG Al A359/ SiCp cylinder for different pressure levels.

The progress of the plastic zone is shown in Fig. 9. The equivalent stresses in the FG Al A359/ SiCp cylinder, and homogenous Al A359 cylinder ( $\sigma_y = 200MPa$ ) are plotted for different  $R_o/R_c$  ratios in the radial direction. It was found that a plastic zone developed from the inner surface. Therefore, pressure  $P_i$  is a function of the plasticity radius ( $R_c$ ).

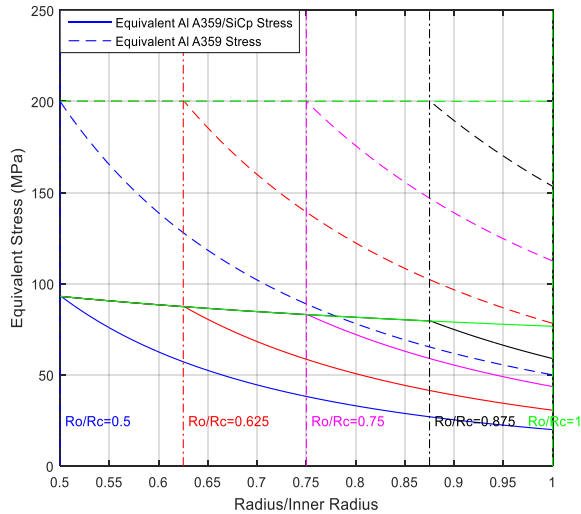


Fig. 9 The advance of the plastic zone for different ratios of FG Al A359/ SiCp cylinder and homogenous Al A359 cylinder.

Fig. 10 and 11 show the residual stresses generated in the FG Al A359/SiCp and homogenous Al A359 cylinders. Both cylinders had already been loaded to pressure  $P_i > P_{lim}$  beyond the elastic range and then unloaded and reloaded with working pressure  $P_w$ . The plastic zone in the FG cylinder is less uniformly distributed; hence, the FG cylinder can resist a higher pressure to become fully plastic.

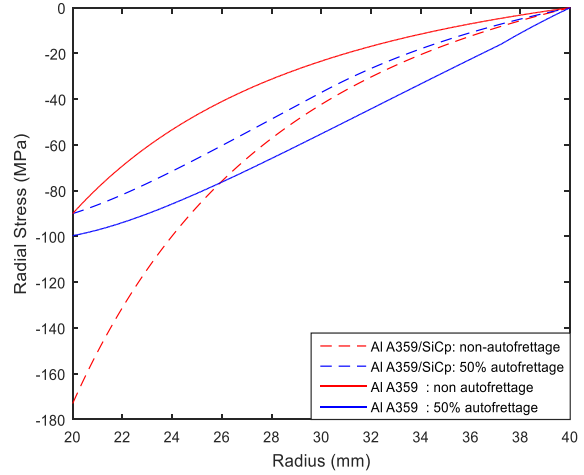


Fig. 10 Radial stress distribution in a self-shrinking FG Al A359/ SiCp cylinder and homogenous Al A359 cylinder.

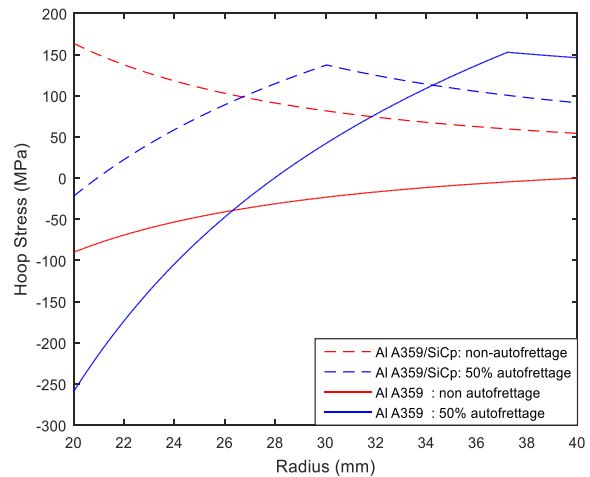


Fig. 11 Hoop stress distribution in an autofrettaged FG Al A359/ SiCp cylinder and homogenous Al A359 cylinder.

The curve shown in Fig. 13, which passes through the maximum values, has a minimum value whose corresponding pressure is the optimal autofrettage pressure.

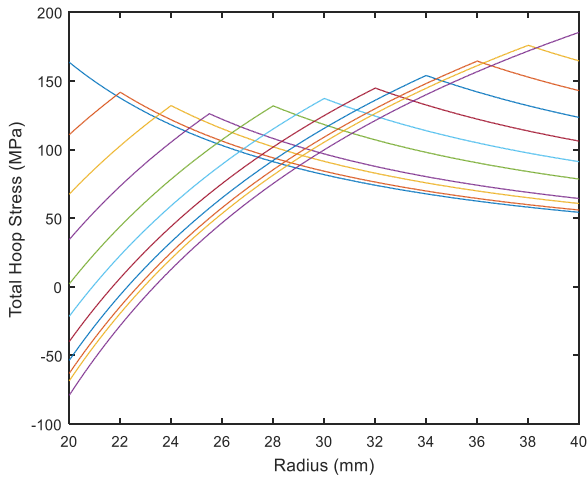


Fig. 12 Variation of total hoop stress for different elasto-plastic boundaries

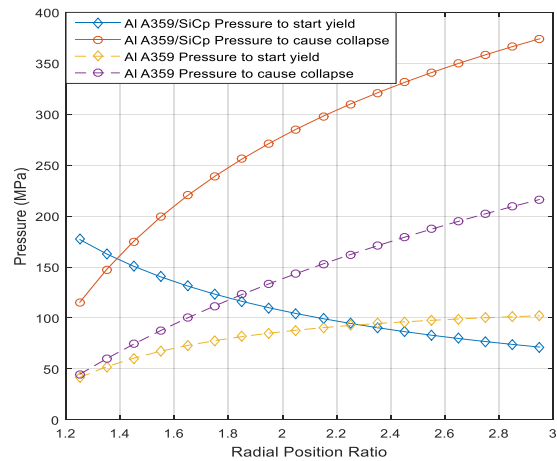


Fig. 14 Variations of the pressure's limit for different ratios of FG Al A359/ SiCp cylinder and homogenous Al A359 cylinder.

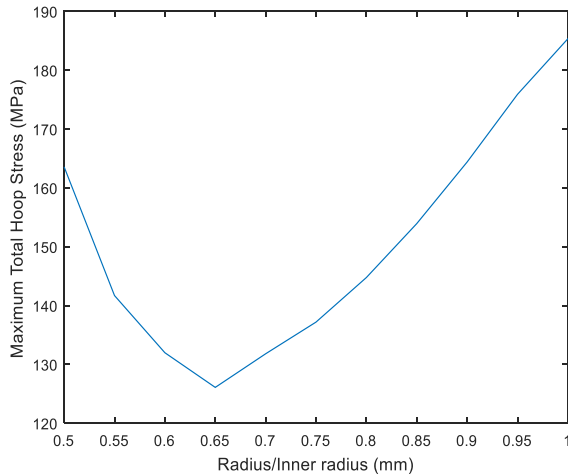


Fig. 13 The envelope curve for several elasto-plastic boundaries going through the points of maximum total hoop stress

The pressure required to start the yield and the pressure required to cause collapse to depend on the material behaviour and geometric characteristics. Fig. 14 shows the variations in these two limiting pressures for different inside-to-outside ratios of the FG Al A359/SiCp and homogenous Al A359 cylinders. For the homogenous cylinder, the thicker the cylinder, the higher the two pressures, and the more significant the difference between the two. However, in the case of the FG Al A359/SiCp, the thicker the cylinder, the lower the pressure to start yielding, and the higher the pressure to cause collapse.

#### 4. Conclusion

In the context of the small-deformation theory and von Mises criteria, this paper presents analytical solutions for the elastic-plastic stress behaviour of a hollow cylinder made of ceramic-metal FGMs under internal and external pressures. New mathematical and numerical methods for analysis under plane strain conditions are presented based on available experimental data for FG Al 359/SiCp. Purely elastic, partially plastic, and fully plastic stress states of the tube were investigated with continuously increasing internal pressure.

As the pressure increased, the yielding region expanded throughout the outer surface of the cylinder. The pressure variation inside the cylindrical tube is a function of plasticity radius; however, the risk of crack evolution is lower for an FG Al A359/SiCp cylinder than for a homogeneous Al A359 cylinder. It is crucial to determine the residual stress level to prevent the rupture of a cylindrical tube before it reaches its elastic limit. The results show that compared with a homogeneous Al A359 cylinder, an FG Al A359/SiCp cylinder exhibits increased load-bearing capacity.

This study is a reference for designing hollow FG Al A359/SiCp cylinders with optimal constituents.

#### Author Contribution Statement

M.B and N.L conceived of the presented idea. M.B developed the theory and performed the computations. N.L and H.B verified the analytical methods. All authors contributed to the analysis of the results and the manuscript's writing.

## References

- [1] Mahamood R. M, & Akinlabi E. T, "Introduction to Functionally Graded Materials," pp. 1–8, 2017.
- [2] Boggarapu V, Gujjala R, Ojha S, Acharya S, Venkateswara Babu P, Chowdary S, & kumar Gara D, "State of the Art in Functionally Graded Materials," *Composite Structures*, vol. 262, pp. 113596, 2021.
- [3] Pasha A, & B.M R, "Functionally Graded Materials (FGM) Fabrication and its Potential Challenges & Applications," *Materials Today: Proceedings*, vol. 52, pp. 413–418, 2022.
- [4] Ibnorachid Z, Boutahar L, & Bikri K., et., "A Refined Theory for Bending Vibratory Analysis of Thick Functionally Graded-Beams," *International Journal of Engineering Trends and Technology*, vol. 69, no. 4, pp. 57–66, 2021. <https://doi.org/10.14445/22315381/IJETT-V69I4P209>.
- [5] Saleh B, Jiang J, Fathi R, Al-hababi T, Xu Q, Wang L, Song D, & Ma A, "30 Years of Functionally Graded Materials: An Overview of Manufacturing Methods, Applications and Future Challenges," *Composites Part B: Engineering*, vol. 201, pp. 108376, 2020.
- [6] Bertolino N, Monagheddu M, Tacca A, Giuliani P, and Zanotti C, "Functionally Graded Materials as Thermal Protection Systems", Hot Structures and Thermal Protection Systems for Space Vehicles, Proceedings of the 4th European Workshop 2002 in Palermo, Italy. Edited by A. Wilson, ESA SP-521, Paris: European Space Agency, pp.155, 2003.
- [7] Zhang X, Chen Y, & Hu J, "Recent Advances in the Development of Aerospace Materials," *Progress in Aerospace Sciences*, vol. 97, pp. 22–34, 2018.
- [8] Hassanzadeh R, & Bilgili M, "Assessment of Thermal Performance of Functionally Graded Materials in Longitudinal Fins," *Journal of Engineering Physics and Thermophysics*, vol. 91, no. 1, pp. 79–88, 2018.
- [9] Yan Z, Huang Q, Guo Z, Song Y, Li C, Liu S, Han Q, & Deng C, "Vacuum Plasma Sprayed FeAl/Al<sub>2</sub>O<sub>3</sub> Functionally Graded Coatings for Fusion Reactor Applications," *Fusion Engineering and Design*, vol. 85, no. 7–9, pp. 1542–1545, 2010.
- [10] Heuer S, Matějčiček J, Vilémová M, Koller M, Illkova K, Veverka J, Weber Th, Pintsuk G, Coenen J. W, & Linsmeier Ch, "Atmospheric Plasma Spraying of Functionally Graded Steel/Tungsten Layers for the First Wall of Future Fusion Reactors," *Surface and Coatings Technology*, vol. 366, pp. 170–178, 2019.
- [11] Chmielewski M, & Pietrzak K, "Metal-Ceramic Functionally Graded Materials – Manufacturing, Characterization, Application," *Bulletin of the Polish Academy of Sciences Technical Sciences*, vol. 64, no. 1, pp. 151–160, 2016. <https://doi.org/10.1515/bpasts-2016-0017>
- [12] Andrew J.Ruys and Brett A.Sutton, "Metal-Ceramic Functionally Graded Materials (FGMs)", *Metal-Reinforced Ceramics*, pp. 327-359, 2021.
- [13] Tutuncu N, & Ozturk M, "Exact Solutions for Stresses in Functionally Graded Pressure Vessels," *Composites Part B: Engineering*, vol. 32, no. 8, pp. 683–686, 2001.
- [14] Sburlati R, "Analytical Elastic Solutions for Pressurized Hollow Cylinders with Internal Functionally Graded Coatings," *Composite Structures*, vol. 94, no. 12, pp. 3592–3600, 2012.
- [15] Benslimane A, Benchallal R, Mammeri S, Methia M, & Khadimallah M. A, "Investigation of Displacements and Stresses in Thick-Walled FGM Cylinder Subjected to Thermo-Mechanical Loadings," *International Journal for Computational Methods in Engineering Science and Mechanics*, vol. 22, no. 2, pp. 138–149, 2021.
- [16] Chen Y. Z, & Lin X. Y, "Elastic Analysis for Thick Cylinders and Spherical Pressure Vessels Made of Functionally Graded Materials," *Computational Materials Science*, vol. 44, no. 2, pp. 581–587, 2008.
- [17] Shi Z, Zhang T, & Xiang H, "Exact Solutions of Heterogeneous Elastic Hollow Cylinders," *Composite Structures*, vol. 79, no. 1, pp. 140–147, 2007. <https://doi.org/10.1016/j.compstruct.2005.11.058>
- [18] Benslimane A, Bouzidi S, & Methia M, "Displacements and Stresses in Pressurized Thick-Walled FGM Cylinders: Exact and Numerical Solutions," *International Journal of Pressure Vessels and Piping*, vol. 168, pp. 219–224, 2018.
- [19] Mognhod Bezzie Y, & Engida Woldemichael D, "Effects of Graded-Index and Poisson's Ratio on Elastic-Solutions of a Pressurized Functionally Graded Material Thick-Walled Cylinder," *Forces in Mechanics*, vol. 4, pp. 100032, 2021. <https://doi.org/10.1016/j.finmec.2021.100032>
- [20] Eraslan NA, Akis T, "Elastoplastic Response of a Long Functionally Graded Tube Subjected to Internal Pressure," *Turkish Journal of Engineering Environmental Sciences*, vol. 29, pp. 361-368, 2005.
- [21] Xin L, Dui G, Yang S, & Liu Y, "Elastic-Plastic Analysis for Functionally Graded Thick-Walled Tube Subjected to Internal Pressure," *Advances in Applied Mathematics and Mechanics*, vol. 8, no. 2, pp. 331–352, 2016. <https://doi.org/10.4208/aamm.2014.m841>

- [22] Nayak P, Bhowmick S, & Saha K. N, "Elasto-Plastic Analysis of Thermo-Mechanically Loaded Functionally Graded Disks by an Iterative Variational Method," *Engineering Science and Technology, An International Journal*, vol. 23, no. 1, pp. 42–64, 2020.
- [23] Heydari, A, "Elasto-Plastic Analysis of Cylindrical Vessel with Arbitrary Material Gradation Subjected to Thermo-Mechanical Loading Via DTM," *Arabian Journal for Science and Engineering*, vol. 44, no. 10, pp. 8875–8891, 2019.
- [24] Saeedi S, Kholdi M, Loghman A, Ashrafi H, & Arefi M, "Thermo-Elasto-Plastic Analysis of Thick-Walled Cylinder Made of Functionally Graded Materials using Successive Approximation Method," *International Journal of Pressure Vessels and Piping*, vol. 194, pp. 104481, 2021.
- [25] Benchallal R, Benslimane A, Bidgoli O, & Hammiche D, "Analytical Solution for Rotating Cylindrical FGM Vessel Subjected to Thermomechanical Loadings," *Materials Today: Proceedings*, vol. 53, pp. 24–30, 2022. <https://doi.org/10.1016/j.matpr.2021.12.212>
- [26] Deepak Ranjan Biswal, Alok Ranjan Biswal, Rashmi Ranjan Senapati, "Finite Element Based Vibration Analysis of an Axially Functionally Graded Nonprismatic Beam," *SSRG International Journal of Mechanical Engineering*, vol. 5, no. 1, pp. 8-13, 2018. Crossref, <https://doi.org/10.14445/23488360/IJME-V5I1P102>
- [27] Sim L. C, Yeo W. H, Purbolaksono J, Saw L. H, & Tey J. Y, "Analytical Solution of Thermo-Mechanical Stresses of Multilayered Hollow Spherical Pressure Vessel," *International Journal of Pressure Vessels and Piping*, vol. 191, pp. 104355, 2021. <https://doi.org/10.1016/j.ijpvp.2021.104355>
- [28] Cui Y, Zhang L, Zhang C, Li R, & Li F, "Stress Analysis of Shrink Fitting Process of Ultra-Thin Reactor Coolant Pump Rotor-Can," *Annals of Nuclear Energy*, vol. 162, pp. 108492, 2021. <https://doi.org/10.1016/j.anucene.2021.108492>
- [29] Zheng M, Ma H, Lyu Y, Lu C, & He C, "Derivation of Circumferential Guided Waves Equations for a Multilayered Laminate Composite Hollow Cylinder by State-Vector and Legendre Polynomial Hybrid Formalism," *Composite Structures*, vol. 255, pp. 112950, 2021. <https://doi.org/10.1016/j.compstruct.2020.112950>
- [30] A M, S J. J, & P B. A, "Fatigue Analysis of Thermal Shrink-Fit Autofrettage in Pressure Cylinder using Finite Element Analysis," *Journal of Materials Research and Technology*, vol. 9, no. 4, pp. 8606–8617, 2020. <https://doi.org/10.1016/j.jmrt.2020.04.021>
- [31] Mohan A, Julyes Jaisingh S, & Goldin Priscilla C. P, "Effect of Autofrettage on the Ultimate Behavior of Thick Cylindrical Pressure Vessels," *International Journal of Pressure Vessels and Piping*, vol. 194, pp. 104546, 2021.
- [32] Molaie M, Darijani H, Bahreman M, & Hosseini S. M, "Autofrettage of Nonlinear Strain-Hardening Cylinders using the Proposed Analytical Solution for Stresses," *International Journal of Mechanical Sciences*, vol. 141, pp. 450–460, 2018.
- [33] R. Rodríguez-Castro, R. C. Wetherhold, and M. H. Kelestemur, "Microstructure and Mechanical Behavior of Functionally Graded Al A359/SiCp Composite", *Material Science and Engineering: A*, vol. 323, pp. 445–456, 2002.
- [34] Vullo V, "Thin-Walled Circular Cylinders Under Internal and/or External Pressure and Stressed in the Linear Elastic Range," *Circular Cylinders and Pressure Vessels*, pp. 1-22, 2013.
- [35] N. Laghzale, A. Bouzid, "Analytical Modelling of Elastic-Plastic Interference Fit Joints," *International Review on Modelling and Simulations (I.R.E.MO.S.)*, vol. 9, no. 3, 2016.
- [36] A.T Kalali S, Hadidi-Moud, "A Semi-Analytical Approach to Elastic-Plastic Stress Analysis of FGM Pressure Vessels," *Journal of Solid Mechanics*, vol. 5, no. 1, pp. 63-73, 2013.
- [37] Bist H, & Bhatt H, "Modeling and Analysis of Crankshaft (Using ANSYS)," *International Journal of Recent Engineering Science*, vol. 8, no. 2, pp. 1–9, 2021. <https://doi.org/10.14445/23497157/IJRES-V8I2P101>
- [38] Parvizi A, Naghdabadi R, & Arghavani J, "Analysis of Al A359/SiCp Functionally Graded Cylinder Subjected to Internal Pressure and Temperature Gradient with Elastic-Plastic Deformation," *Journal of Thermal Stresses*, vol. 34, no. 10, pp. 1054–1070, 2011.